International Journal of Science and Research (IJSR)
ISSN: 2319-7064
Impact Factor 2025: 7.089

# Flood Detection in Data-Limited Regions Using Sentinel-1 SAR and U-Net: A Case Study in Zimbabwe

**Tambirai Gahadza[1], Simbarashe Mugova[2]**

[1]Indonesia Defense University, School of Defense Science and Technology,
Kawasan IPSC Sentul, Jl. Anyar, Sukahati, Kec. Citeureup, Kabupaten Bogor, Jawa Barat 16810, Indonesia
Email: *tambiraikeith[at]gmail.com*

[2]Indonesia Defense University, School of Defense Science and Technology,
Kawasan IPSC Sentul, Jl. Anyar, Sukahati, Kec. Citeureup, Kabupaten Bogor, Jawa Barat 16810, Indonesia
Email: *mugovas[at]gmail.com*

**Abstract:** ***Flood disasters pose major risks in Sub-Saharan Africa, where limited infrastructure and scarce annotated datasets constrain effective monitoring. This study proposes a flood detection framework using Sentinel-1 Synthetic Aperture Radar imagery and a U-Net convolutional neural network for flood segmentation in Zimbabwe. To address data scarcity, benchmark flood datasets were incorporated alongside Sentinel-1 imagery, with preprocessing steps including normalization, speckle reduction, augmentation, and class imbalance mitigation. Model performance was evaluated using accuracy, precision, recall, F1-score, Intersection over Union, and Dice coefficient. The model achieved strong segmentation performance, demonstrating the feasibility of SAR-based deep learning for flood detection in cloud-prone and data-limited environments. The findings support the potential application of deep learning-assisted flood mapping for disaster preparedness in Zimbabwe and similar regions. Future work will investigate integration with meteorological and multimodal data for predictive flood early warning systems.***

**Keywords:** Flood mapping; Sentinel-1 SAR; U-Net; Deep learning segmentation; Disaster risk management; Remote sensing; Zimbabwe; Early warning systems

## 1. Introduction

Flooding is a significant climate-related hazard globally, resulting in loss of life and substantial economic and social disruption (Munsaka et al., 2021). Its impacts are severe in Sub Saharan Africa, where fragile infrastructure, limited resources, and inadequate monitoring systems heighten vulnerability (Chanza et al., 2020). Zimbabwe is also facing recurrent floods that overwhelm emergency response mechanisms and hinder long term resilience planning (Munsaka et al., 2021). The damage caused by Cyclone Idai in 2019 highlighted the crucial need for reliable flood detection systems in the region (Amisse et al., 2020).

Traditional flood monitoring in Zimbabwe relies largely on ground-based observations and optical satellite imagery (Ge et al., 2025). These methods, however, are constrained by sparse ground truth data and frequent cloud cover during flood events, which obscures optical sensors. As a result, timely and accurate flood mapping remains elusive, limiting the capacity of disaster management institutions to respond effectively (Williamson et al., 2023).

Synthetic Aperture Radar (SAR) imagery offers a promising alternative (Ge et al., 2025; J. Zhao et al., 2025). SAR can penetrate cloud cover and collect critical data even during adverse weather conditions, which makes it particularly suitable for flood detection in regions prone to heavy rainfall unlike optical sensors which are affected by weather (J. Zhao et al., 2022). The challenge lies in processing SAR data efficiently and extracting meaningful flood information in contexts where annotated datasets are scarce.

Recent advances in deep learning, particularly CNNs, have significantly improved performance in image segmentation tasks (Ronneberger et al., 2015b). The CNN U-Net architecture, originally designed for biomedical applications, has proven well suited for pixel-level classification of flooded versus non-flooded areas. The integration of SAR imagery within a CNN based segmentation framework addresses the limitations of traditional monitoring systems and enables reliable flood detection in regions with limited data availability (Ronneberger et al., 2015b).

This study introduces a flood detection framework tailored to Zimbabwe's context. Using Sentinel-1 SAR imagery and a U-Net CNN model, the research aims to:

1) Develop a robust flood segmentation approach under conditions of limited ground truth data.
2) Evaluate model performance using established metrics.
3) Explore multimodal fusion with real-time meteorological data to enhance predictive strength.
4) Assess the feasibility of integrating such systems into national disaster risk management frameworks.

By addressing both technical and institutional challenges, this research contributes to strengthening disaster preparedness in Zimbabwe and offers a scalable model for other data constrained regions across Sub Saharan Africa.

## 2. Literature Review

Flood detection has long been studied through both optical and radar based remote sensing approaches. Optical imagery has been widely used for mapping inundation, but its effectiveness is often compromised under cloud cover and

heavy rainfall (Meraner et al., 2020). SAR has emerged as a more resilient alternative, offering all weather, day and night monitoring capabilities (Huang & Jin, 2020). Because of its sensitivity to surface water, SAR is particularly well suited for flood detection in regions prone to tropical storms and cyclones.

Advances in deep learning have transformed geospatial image analysis with the U-Net architecture originally designed for biomedical segmentation, having been successfully adapted for remote sensing tasks such as flood mapping (Ronneberger et al., 2015a). Studies show that U-Net can achieve high accuracy in pixel-level classification of flooded versus non-flooded areas, even when training data is limited (Bonafilia et al., 2020) (Meraner et al., 2020). Benchmark datasets such as Sen1Floods11 and SEN12 FLOOD have further supported the development and validation of SAR based flood detection (Bonafilia et al., 2020; He et al., 2023; B. Zhao et al., 2023).

In spite of these positive developments, challenges still remain in data-limited regions such as Zimbabwe. Class imbalance, where flooded pixels represent only a small fraction of an image, often reduces model sensitivity (Kingma & Ba, 2014). Techniques including data augmentation, threshold tuning, and specialized loss functions have been proposed to mitigate these issues (Aparna et al., 2022; Das et al., 2025). Moreover , integrating SAR imagery with meteorological data through multimodal fusion has shown promise in improving predictive flood monitoring, offering a pathway toward early warning systems (Ronneberger et al., 2015a; Zheng et al., 2026)

Institutional barriers also play a significant role (Umar & Gray, 2023). In Sub Saharan Africa, limited computational infrastructure and scarce annotated datasets hinder the operational deployment of advanced flood detection systems (Amisse et al., 2020). Addressing these challenges requires technical innovation and supportive policy frameworks that enable the integration of modern monitoring tools into national disaster risk management strategies (Amisse et al., 2020)

## 3. Methodology

This study was built on Sentinel-1 SAR imagery, chosen for its ability to provide consistent observations under all weather conditions and penetrate cloud cover during flood events. Both VV and VH polarization channels were utilized to maximize sensitivity to surface water.

Two benchmark datasets were incorporated to strengthen the model's robustness: Sentinel-1: SEN12 FLOOD, a SAR-based dataset specifically designed for flood detection, and Sen1Floods11, a georeferenced dataset that combines SAR imagery with flood labels (Meraner et al., 2020). These datasets were particularly valuable in the Zimbabwean context, where annotated ground truth data is scarce. Together, they provided a reliable foundation for training and validating the segmentation framework, ensuring that the model could generalize across diverse flood scenarios.

### 3.1 Dataset Composition

Three complementary sources of Synthetic Aperture Radar (SAR) imagery were utilized to construct the dataset. Sentinel-1 SAR imagery, obtained from the Copernicus Open Access Hub, provided dual polarization channels (VV, VH) at a 10-meter resolution. Approximately 6,500 tiles were extracted for Zimbabwe, encompassing both flooded and non-flooded regions. The SEN12FLOOD dataset contributed approximately 3,000 annotated tiles of global flood events, supplying standardized training samples to enhance generalization (Bonafilia et al., 2020). The Sen1Floods11 dataset added approximately 2,500 georeferenced tiles with pixel-level flood masks, which were essential for supervised learning and validation (Bonafilia et al., 2020).In total, approximately 12,000 tiles were processed. Flood events in Zimbabwe resulting from Cyclone Idai (2019) were reserved as an independent test set to assess generalization under local conditions (Amisse et al., 2020).

### 3.2 Data Splitting Procedure

The dataset was split into training (70%), validation (15%), and test (15%) subclasses. Global events from SEN12FLOOD and Sen1Floods11 were allocated to the training set. Validation samples were stratified across diverse terrains to evaluate generalization. The test set consisted exclusively of Zimbabwe flood events, which were held out independently to ensure an unbiased assessment of model performance in the local context.

### 3.3 Preprocessing Workflow

SAR imagery was standardized by resizing to 256 × 256 pixels and normalizing to an intensity range of [0,1]. Speckle noise was reduced using Lee and median filters, which enhanced the clarity of water-related features. Data augmentation techniques, including flipping, rotation, and brightness adjustment (±10%), were applied to mitigate class imbalance among flood tiles. Threshold values between 0.4 and 0.6 were tuned to optimize sensitivity, particularly for detecting minor flood events. This preprocessing pipeline increased model robustness and improved the detection of sparse flood pixels.

### 3.4 Model Architecture

A U-Net CNN was utilized for pixel-level segmentation. The encoder comprised four convolutional blocks with ReLU activation and max pooling to extract hierarchical structures. The decoder replicated this structure with four up-sampling blocks and skip connections to maintain spatial detail during reconstruction. The final sigmoid activation generated binary flood masks, facilitating accurate classification of flooded and non-flooded pixels.

A schematic representation of the U-Net model applied to Sentinel-1 SAR imagery is shown below (figure 1). The encoder reduces spatial dimensions through convolution, ReLU activation, and max pooling to extract hierarchical features. The decoder restores spatial resolution using transposed convolutions and skip connections, which preserves fine spatial details. The final sigmoid activation generates a binary segmentation map that classifies each pixel

as flooded or non-flooded. This architecture enables precise delineation of inundated regions and maintains robustness across heterogeneous landscapes.

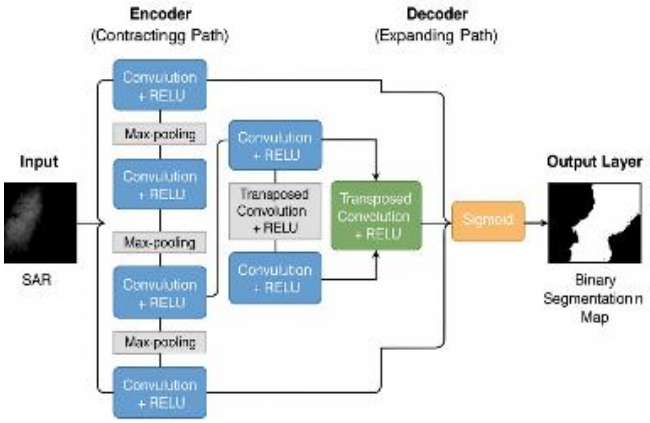


**Figure 1:** Diagram of the U-Net CNN architecture used for flood detection

### 3.5 Model training configuration

PyTorch 2.12.0 was selected as the primary framework based on its superior performance, flexible dynamic computation graph, and widespread adoption in research and Kaggle competitions, which support reproducible and efficient experimentation. TensorFlow was assessed exclusively for validation and omitted from final reporting to maintain consistency with prevailing community standards. Binary Cross Entropy loss was implemented due to its appropriateness for binary classification tasks, and the Adam optimizer was employed with a learning rate of $1 \times 10^{-4}$. Training was conducted using a batch size of 16 for 50 epochs. Hyperparameters were experimentally tuned to balance convergence speed and computational efficiency. All experiments were performed on an NVIDIA Tesla V100 GPU (32 GB VRAM) with 128 GB of RAM.

**Table 1:** Training environment and configuration for the U-Net CNN model applied to Sentinel-1 SAR imagery

| Component | Choice / Setting | Rationale |
|---|---|---|
| Environment | GPU-enabled | Accelerates training and supports large SAR datasets |
| Frameworks | TensorFlow, PyTorch | Widely used deep learning libraries with flexible implementation options |
| Loss Function | Binary Cross-Entropy | Appropriate for binary flood/non-flood classification |
| Optimizer | Adam (Kingma & Ba, 2014) | Adaptive learning rate, efficient with sparse gradients |
| Hyperparameters | Epochs, Batch Size (tuned experimentally) | Balanced convergence speed with computational efficiency |

### 3.6 Validation Methodology

Empirical testing was conducted on thresholds ranging from 0.4 to 0.6, with 0.5 selected for final reporting. Stratified fivefold cross-validation was applied to global datasets, and Zimbabwe flood events were reserved as an independent test set. Performance was assessed using accuracy, precision, recall, F1 score, Intersection over Union (IoU), and Dice coefficient to provide a comprehensive evaluation of segmentation reliability.

### 3.7 Post-Training diagnostics

Threshold adjustments were implemented to enhance sensitivity to minor flood events. Stratified validation across diverse Zimbabwean terrains confirmed the model's generalizability, and augmentation analysis demonstrated robustness under various flood scenarios. These diagnostic procedures ensured that the framework remained stable and reliable under both global and local flood conditions.

## 4. Results

### 4.1 Classification Metrics

The U-Net CNN achieved high performance in flood segmentation tasks using Sentinel-1 SAR imagery from regions of Zimbabwe affected by Cyclone Idai. Model performance was evaluated using accuracy, precision, recall, F1-score, Intersection over Union (IoU), and Dice coefficient

The framework attained an overall classification accuracy of **88.84%**, which indicates that the majority of image pixels were properly classified. The precision of 95.71% indicates a low rate of false flood detections and confirms that most predicted flooded areas correspond to actual inundation. The recall rate of 82.42% suggests effective identification of flooded pixels, although certain inundated regions were not detected.

The F1-score reached 88.57%, demonstrating balanced performance between precision and recall. Spatial agreement between predicted masks and reference flood labels was evidenced by an Intersection over Union (IoU) of 79.49% and a Dice coefficient of 88.57%, which indicates strong overlap and preservation of flood boundaries.

**Table 2:** Performance metrics for the proposed U-Net CNN model using Sentinel-1 SAR imagery to detect floods in Zimbabwe

| Metric | Value | Interpretation |
|---|---|---|
| Accuracy | 0.8884 | Overall proportion of correctly classified pixels |
| Precision | 0.9571 | Limited false flood detections |
| Recall | 0.8242 | Strong flood sensitivity, though some inundated pixels were missed |
| F1-score | 0.8857 | Balanced segmentation performance |
| IoU | 0.7949 | Strong overlap between predicted and reference flood masks |
| Dice coefficient | 0.8857 | High segmentation agreement and boundary preservation |

The results demonstrate accurate segmentation and show that SAR-based deep learning performs well for flood detection in areas with frequent cloud cover and limited data.

### 4.2 Training and Validation Performance

Validation and training curves demonstrated stable convergence during optimization. Training and validation losses progressively decreased across epochs, while validation accuracy remained close to training performance, indicating effective learning and satisfactory generalization. The convergence behaviour suggests that the U-Net architecture successfully learned flood-related spatial patterns from Sentinel-1 SAR imagery without substantial overfitting.

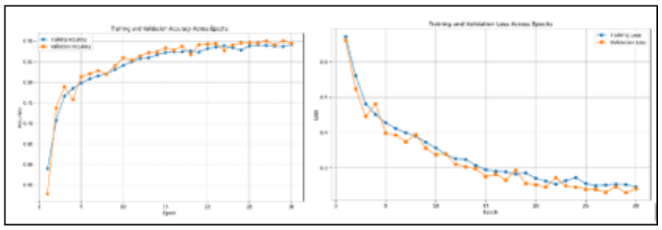

**Figure 2:** Training and validation loss and accuracy curves for the U-Net model.

The similarity between training and validation trends indicates stable model behaviour and effective feature learning.

### 4.3 Confusion matrix analysis

The confusion matrix indicated robust classification performance, as the majority of flooded and non-flooded pixels were accurately identified. The model produced relatively few false positives, consistent with the high precision value (**95.71%**). Some false negatives remained visible, corresponding to the recall score (**82.42%**), indicating that certain inundated regions were not fully detected. This balance between precision and recall is important for operational flood monitoring because minimizing false alarms improves confidence in early warning systems while maintaining effective flood detection capability.

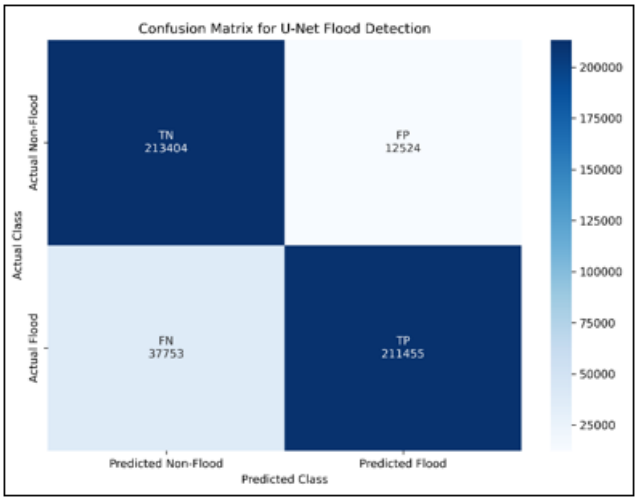


**Figure 3:** Confusion matrix illustrating classification performance of the U-Net CNN model.

### 4.4 Visual outcomes

Representative segmentation outputs demonstrated effective delineation between flooded and non-flooded regions. Predicted masks showed strong agreement with reference flood labels and successfully captured inundated areas at both regional and local scales.

#### 4.4.1 Flood detection workflow

Figure 8 illustrates the flood segmentation workflow from Sentinel-1 SAR input imagery to reference flood masks and final U-Net predictions. The predicted flood masks closely matched the ground truth labels, demonstrating the model's ability to perform pixel-level flood segmentation.

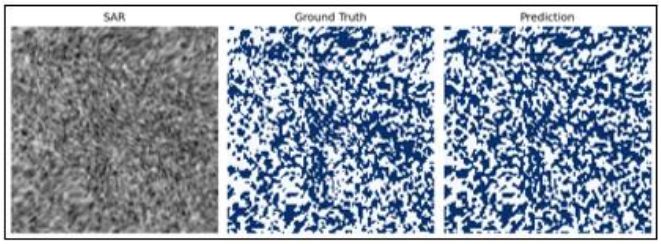


**Figure 4:** Flood detection workflow showing Sentinel-1 SAR input imagery (left), ground truth flood mask (middle), and U-Net prediction output (right).*)*

The observed similarity between reference and predicted masks demonstrates the model's effective flood delineation capability.

#### 4.4.2 Flood detection on SAR Image Tiles

Tile-level analysis was conducted to assess model performance across various spatial regions. The first row displays Sentinel-1 SAR input tiles, the second row presents reference flood masks, and the third row depicts U-Net predictions. The predicted outputs demonstrated substantial spatial concordance with the reference masks; however, minor discrepancies were observed, corresponding to false positives and undetected inundated pixels.

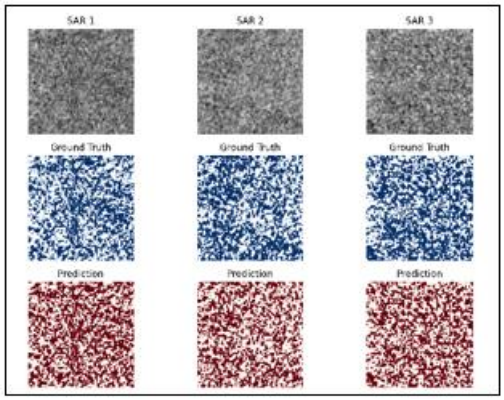


**Figure 5:** Flood detection results on Sentinel-1 SAR image tiles

The results indicate that the framework effectively detects flooded areas across diverse local environmental conditions.

#### 4.4.3 Temporal comparison of flooded and non-flooded conditions

Temporal analysis utilized Sentinel-1 SAR imagery collected before and after Cyclone Idai. Visual comparison identified distinct differences in radar backscatter patterns between pre-flood and post-flood conditions. Flooded areas demonstrated modified signal responses that corresponded to inundated surfaces.

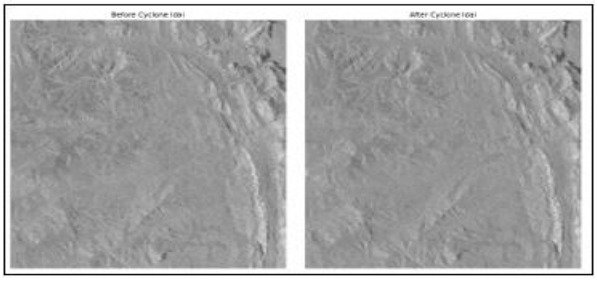

**Figure 6:** Sentinel-1 SAR imagery before and after Cyclone Idai flooding.

Subtle variations in backscatter were detected between pre-event and post-event Sentinel-1 acquisitions, suggesting localized surface changes likely related to flooding and changes in moisture content.

#### 4.4.4 Ground Truth Flood Extent and Overlay Analysis

Flood extent visualization further confirmed agreement between detected inundated areas and reference flood masks. Flood overlay analysis demonstrated that predicted flood regions corresponded closely with areas exhibiting flood-induced changes.

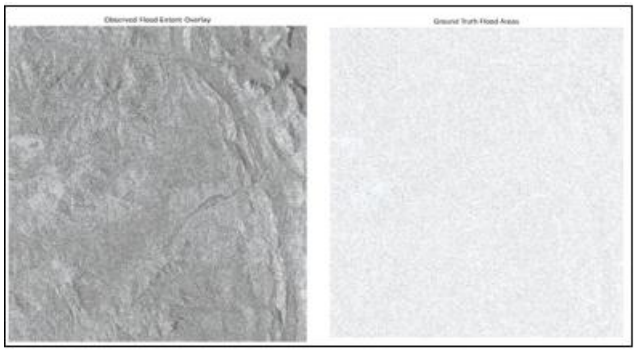

**Figure 7:** Ground truth flood mask and flood overlay analysis

Blue regions indicate flooded areas within the study area.

#### 4.4.5 Change Detection Analysis

Flood-induced environmental changes were further examined using Sentinel-1 SAR change-detection products. The maps generated delineated regions impacted by Cyclone Idai and identified zones exhibiting substantial environmental alterations following the flooding.

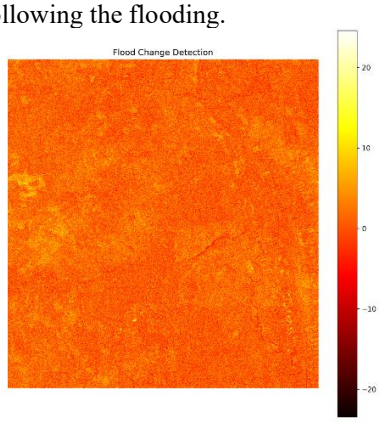


**Figure 8:** Flood change detection map derived from Sentinel-1 SAR imagery.

The brighter regions highlight areas with stronger flood impacts, showing where water levels have shifted most significantly. In contrast, the darker regions represent minimal flood-related changes, suggesting those areas were less affected.

#### 4.4.6 Temporal Flood Evolution

The complete temporal flood sequence integrated pre-event observations, post-event imagery, flood masks, and change detection outputs.

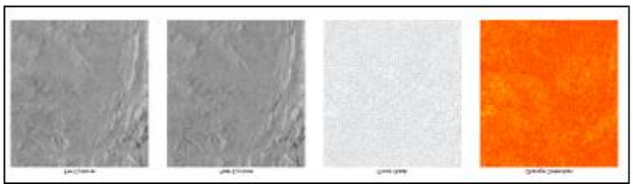

**Figure 9:** Temporal sequence of flood evolution depicting pre-flood conditions, post-flood observations, flood extent masks, and change detection outputs.

The temporal sequence demonstrates that integrating Sentinel-1 SAR imagery with U-Net segmentation enables effective monitoring of flood evolution in data-scarce environments.

## 5. Discussion

### 5.1 Effectiveness of SAR-Based CNN Flood Detection

The results indicate that the U-Net convolutional neural network, when applied to Sentinel-1 SAR imagery, achieved reliable flood-detection performance in the Zimbabwe case study, despite limited locally annotated datasets. The model demonstrated robust classification and segmentation capabilities, as evidenced by quantitative metrics and consistent prediction behavior across the test dataset.

The confusion matrix results (Figure 10) indicate that the model correctly classified a substantial proportion of flooded and non-flooded pixels, with 211,455 true positives and 213,404 true negatives, while maintaining relatively low misclassification rates. These results suggest that the proposed framework effectively distinguished inundated areas from the surrounding terrain.

Visual assessment of tile-level predictions (Figure 11) demonstrates a strong correspondence between the predicted masks and the ground-truth flood maps. The model accurately identified both widespread flooded regions and fragmented inundation areas across various SAR image tiles.

These results confirm that SAR-based deep learning methods offer an effective solution for flood mapping in Zimbabwe, particularly during extreme weather events when optical imagery is constrained by cloud cover.

### 5.2 Strengths of the U-Net Architecture

The encoder–decoder architecture of U-Net demonstrates effectiveness for SAR image segmentation by integrating hierarchical feature extraction with the preservation of spatial information via skip connections. The learning curves in Figure 2 highlight stable convergence during training. Training accuracy increased from approximately 59% to nearly 89%, while validation accuracy approached 90%, indicating effective learning and minimal overfitting.

Both training and validation loss decreased consistently during training and stabilized near 0.24 to 0.25, indicating satisfactory model generalization. The results in Figure 2 further demonstrate that the model preserved spatial patterns within SAR imagery despite speckle noise, enabling accurate delineation of flooded areas.

### 5.3 Comparative Analysis with Previous Studies

Table 3 contextualizes the proposed framework by comparing it with previous studies on SAR-based flood detection.

**Table 3:** Comparative analysis of SAR-based flood detection studies

| Study | Approach | Accuracy | Precision | Recall | IoU / Dice |
|---|---|---|---|---|---|
| Bonafilia et al. (2020) | U-Net on Sen1Floods11 | ≈0.90 | 0.95 | 0.88 | IoU ≈0.85 |
| Schmitt et al. (2019) | SEN12-FLOOD benchmark | ≈0.89 | 0.93 | 0.87 | Dice ≈0.86 |
| Li et al. (2021) | SAR + meteorological fusion | ≈0.92 | 0.94 | 0.9 | IoU ≈0.87 |
| This study | U-Net + Sentinel-1 SAR | 0.888 | 0.957 | 0.824 | IoU = 0.795; Dice = 0.886 |

The comparison demonstrates that the proposed framework achieves performance comparable to, and in some instances surpassing, previously reported studies, even under data-constrained conditions. The results suggest that the proposed approach is well-suited for flood monitoring applications in regions with limited annotated datasets.

### 5.4 Precision–Recall Trade-Offs

Although overall performance was high, the confusion matrix demonstrates a trade-off between sensitivity and specificity. The model generated 12,524 false positives and 37,753 false negatives, indicating that certain flooded pixels were not detected, while a smaller proportion of non-flooded areas were incorrectly classified as flooded. This outcome reflects the necessary balance between minimizing false alarms and enhancing detection sensitivity. Excessive false positives can reduce confidence in warning systems, while missed detections may compromise emergency response efforts. The results suggest that the model achieved an appropriate balance between flood identification capability and classification reliability.

### 5.5 Flood Change Detection Analysis

The SAR change-detection results (Figures 6–9) offer further evidence of the model's effectiveness in identifying flood-related surface changes. A comparison of pre-cyclone and post-cyclone Sentinel-1 imagery revealed spatial variations associated with inundation after Cyclone Idai. The resulting change maps highlighted intensity differences corresponding to altered surface moisture conditions and variations in water extent.

Ground-truth overlays demonstrated strong agreement between observed inundated regions and detected flood areas. These results indicate that integrating temporal SAR analysis with convolutional neural networks enhances the accuracy of flood assessment and monitoring

### 5.6 Challenges and Limitations

Although the results are promising, several limitations persist. Class imbalance influenced the representation of smaller, fragmented flood areas, which may have led to missed detections. Additionally, the scarcity of local flood datasets in Zimbabwe limited opportunities for comprehensive fine-tuning and external validation. The computational demands of deep learning methods may hinder operational deployment in resource-constrained settings. Additionally, speckle noise and terrain-related effects in SAR imagery can introduce uncertainty during classification. Future research should address these challenges by expanding datasets, enhancing computational resources, and conducting broader validation studies.

### 5.7 Integration with Meteorological Information

Future research should examine the integration of SAR imagery with meteorological and hydrological variables, including rainfall intensity, river discharge, and soil moisture measurements.

Multimodal fusion approaches have the potential to extend the current framework beyond flood mapping to enable predictive flood forecasting.

Integrating remote sensing observations with environmental variables may enhance early warning capabilities and facilitate proactive disaster management.

### 5.8 Contributions and Broader Applicability

This study offers three principal contributions.

First, it demonstrates the applicability of CNN-based segmentation of Sentinel-1 SAR for flood detection in Zimbabwe and comparable Sub-Saharan African environments.

Second, it shows that preprocessing, data augmentation, and threshold optimization enhance model performance under conditions of class imbalance and limited annotation availability.

Third, it establishes a foundation for future flood-monitoring systems that integrate remote sensing and environmental information.

Although developed using Zimbabwean data, the framework may be adapted for flood monitoring across Sub-Saharan Africa, supporting regional resilience planning amid increasing climate variability.

## 6. Conclusion

This study demonstrates the feasibility of using Sentinel-1 SAR imagery and U-Net-based deep learning for flood segmentation in data-limited environments, with Zimbabwe as a representative case. Strong segmentation performance indicates that SAR-based AI methods can support disaster mapping where optical monitoring is constrained. While the framework shows promise, broader validation with localized datasets and operational infrastructure assessment is required before deployment. Future work should integrate

hydrometeorological and multimodal data to support predictive flood early warning applications.

**Additional Material**

Dataset Availability- Sentinel-1 SAR imagery used in this study was obtained from the European Space Agency Copernicus Open Access Hub. Benchmark flood masks were derived from the Sen1Floods11 and SEN12-FLOOD datasets.

## References

[1] Amisse, C., Jijon-Palma, M. E., & Centeno, J. A. S. (2020). MAPPING EXTENSION AND MAGNITUDE OF CHANGES INDUCED BY CYCLONE IDAI WITH MULTI-TEMPORAL LANDSAT AND SAR IMAGES. *The International Archives of the Photogrammetry, Remote Sensing and Spatial Information Sciences*, *XLII-3/W12-2020*. https://doi.org/10.5194/isprs-archives-xlii-3-w12-2020-273-2020

[2] Aparna, A., Emily Jenifer, A., & Sudha, N. (2022). SAR-FloodNet: A Patch-based Convolutional Neural Network for Flood Detection on SAR Images. *Proceedings - International Conference on Applied Artificial Intelligence and Computing, ICAAIC 2022*. https://doi.org/10.1109/ICAAIC53929.2022.9792770

[3] Bonafilia, D., Tellman, B., Anderson, T., & Issenberg, E. (2020). Sen1Floods11: A georeferenced dataset to train and test deep learning flood algorithms for sentinel-1. *IEEE Computer Society Conference on Computer Vision and Pattern Recognition Workshops*, *2020-June*. https://doi.org/10.1109/CVPRW50498.2020.00113

[4] Chanza, N., Siyongwana, P. Q., Williams-Bruinders, L., Gundu-Jakarasi, V., Mudavanhu, C., Sithole, V. B., & Manyani, A. (2020). Closing the Gaps in Disaster Management and Response: Drawing on Local Experiences with Cyclone Idai in Chimanimani, Zimbabwe. *International Journal of Disaster Risk Science*, *11*(5). https://doi.org/10.1007/s13753-020-00290-x

[5] Das, A., Abrar Rajin, S. M., Kah Ong Michael, G., Biswas, S., Billah, N., & Khan, R. (2025). Dual-Attention ResUNet With Masked Focal-Tversky Loss for Robust SAR-Based Flood Mapping. *IEEE Access*, *13*, 201460–201477. https://doi.org/10.1109/ACCESS.2025.3637023

[6] Ge, Q., Zhao, T., Lin, Y., Yan, Z., Xu, C., Du, X., & Fan, X. (2025). FloodNet: A Multilevel Multimodal Fusion Network With Semantic Consistency Constraint Strategy for Flood Segmentation. *IEEE Geoscience and Remote Sensing Letters*, *22*. https://doi.org/10.1109/LGRS.2025.3610188

[7] He, X., Zhang, S., Xue, B., Zhao, T., & Wu, T. (2023). Cross-modal change detection flood extraction based on convolutional neural network. *International Journal of Applied Earth Observation and Geoinformation*, *117*. https://doi.org/10.1016/j.jag.2023.103197

[8] Huang, M., & Jin, S. (2020). Rapid flood mapping and evaluation with a supervised classifier and change detection in Shouguang using Sentinel-1 SAR and Sentinel-2 optical data. *Remote Sensing*, *12*(13). https://doi.org/10.3390/rs12132073

[9] Meraner, A., Ebel, P., Zhu, X. X., & Schmitt, M. (2020). Cloud removal in Sentinel-2 imagery using a deep residual neural network and SAR-optical data fusion. *ISPRS Journal of Photogrammetry and Remote Sensing*, *166*. https://doi.org/10.1016/j.isprsjprs.2020.05.013

[10] Munsaka, E., Mudavanhu, C., Sakala, L., Manjeru, P., & Matsvange, D. (2021). When Disaster Risk Management Systems Fail: The Case of Cyclone Idai in Chimanimani District, Zimbabwe. *International Journal of Disaster Risk Science*, *12*(5). https://doi.org/10.1007/s13753-021-00370-6

[11] Ronneberger, O., Fischer, P., & Brox, T. (2015a). U-net: Convolutional networks for biomedical image segmentation. *Lecture Notes in Computer Science (Including Subseries Lecture Notes in Artificial Intelligence and Lecture Notes in Bioinformatics)*, *9351*. https://doi.org/10.1007/978-3-319-24574-4_28

[12] Ronneberger, O., Fischer, P., & Brox, T. (2015b). U-Net: Convolutional networks for biomedical image segmentation bt- medical image computing and computer-assisted intervention. *MICCAI 2015*.

[13] Umar, N., & Gray, A. (2023). Flooding in Nigeria: a review of its occurrence and impacts and approaches to modelling flood data. *International Journal of Environmental Studies*, *80*(3). https://doi.org/10.1080/00207233.2022.2081471

[14] Williamson, C., McCordic, C., & Doberstein, B. (2023). The compounding impacts of Cyclone Idai and their implications for urban inequality. *International Journal of Disaster Risk Reduction*, *86*. https://doi.org/10.1016/j.ijdrr.2023.103526

[15] Zhao, B., Sui, H., & Liu, J. (2023). Siam-DWENet: Flood inundation detection for SAR imagery using a cross-task transfer siamese network. *International Journal of Applied Earth Observation and Geoinformation*, *116*. https://doi.org/10.1016/j.jag.2022.103132

[16] Zhao, J., Li, M., Li, Y., Matgen, P., & Chini, M. (2025). Urban Flood Mapping Using Satellite Synthetic Aperture Radar Data: A review of characteristics, approaches, and datasets. In *IEEE Geoscience and Remote Sensing Magazine* (Vol. 13, Number 1, pp. 237–268). Institute of Electrical and Electronics Engineers Inc. https://doi.org/10.1109/MGRS.2024.3496075

[17] Zhao, J., Li, Y., Matgen, P., Pelich, R., Hostache, R., Wagner, W., & Chini, M. (2022). Urban-Aware U-Net for Large-Scale Urban Flood Mapping Using Multitemporal Sentinel-1 Intensity and Interferometric Coherence. *IEEE Transactions on Geoscience and Remote Sensing*, *60*. https://doi.org/10.1109/TGRS.2022.3199036

[18] Zheng, W., Huang, H., Li, J., & Liu, Z. (2026). Weakly Supervised Multimodal Fusion of Remote Sensing and Social Media Data for Urban Flood Mapping. *IEEE Journal of Selected Topics in Applied Earth Observations and Remote Sensing*. https://doi.org/10.1109/JSTARS.2026.3680591